Density-functional model for van der Waals interactions: Unifying atomic approaches with nonlocal functionals

Jan Hermann[1,2,*] and Alexandre Tkatchenko[1,*]

[1] *Physics and Materials Science Research Unit, University of Luxembourg, L-1511 Luxembourg City, Luxembourg*
[2] *FU Berlin, Department of Mathematics and Computer Science, Arnimallee 6, 14195 Berlin, Germany*

Abstract Noncovalent van der Waals (vdW) interactions are responsible for a wide range of phenomena in matter. Popular density-functional methods that treat vdW interactions use disparate physical models for these intricate forces, and as a result the applicability of existing methods is often restricted to a subset of relevant molecules and materials. Aiming towards a general-purpose density functional model of vdW interactions, here we unify two complementary approaches: nonlocal vdW functionals for polarization and interatomic methods for many-body interactions. The developed nonlocal many-body dispersion method (MBD-NL) increases the accuracy and efficiency of existing vdW functionals and is shown to be broadly applicable to molecules, soft and hard materials including ionic and metallic compounds, as well as organic/inorganic interfaces.

The van der Waals (vdW) interactions originate from nonlocal correlations in the quantum motion of electrons and give rise to a wide spectrum of physical phenomena ranging from attraction between two atoms (London, 1930) to the macroscopic Casimir effect (Jaffe, 2005). As a result, vdW interactions are one of the prime targets in material modeling, which has led to a plethora of approaches that either treat vdW forces on the same footing as the rest of electron correlation or model them with effective potentials (Klimeš and Michaelides, 2012; Grimme et al., 2016; Hermann et al., 2017). They include quantum Monte–Carlo (QMC) (Ambrosetti et al., 2014a), the coupled cluster method (Yang et al., 2014), random-phase approximation (Lu et al., 2009), nonlocal density functionals (Dion et al., 2004; Vydrov and Van Voorhis, 2009), and coarse-grained approaches, which range from pairwise (Grimme et al., 2010; Becke and Johnson, 2007; Tkatchenko and Scheffler, 2009) to many-body models (Tkatchenko et al., 2012; Silvestrelli, 2013; Caldeweyher et al., 2019).

From a theoretical perspective, this status quo is undesirable, because different models give often disparate pictures of the nature of vdW forces, which leads to incoherent understanding of vdW interactions in molecules and materials. From a practical perspective, the three main characteristics of a method are its generality, accuracy, and computational efficiency, and so far, no single method has satisfied all these three requirements while being applicable to all the relevant types of matter. For instance, QMC and coupled cluster are limited by computational efficiency, pairwise approaches and two-point vdW functionals lack in accuracy for nanostructured and supramolecular compounds, and atomic models have qualitative problems with description of ionic and hybrid metal-organic systems.

In this work, we present a unified density-functional model of vdW interactions that couples polarizability density functionals and atomic models, inheriting broad applicability of the former and excellent accuracy of the latter. We integrate the polarizability functional of Vydrov and Van Voorhis (2010b) (VV), normalization to reference free-atom vdW parameters of the Tkatchenko–Scheffler (TS) model (Tkatchenko and Scheffler, 2009), normalization to jellium via a zero-gradient limit from the VV10 nonlocal functional (Vydrov and Van Voorhis, 2010a), and the Hamiltonian form for the dispersion energy of the many-body dispersion (MBD) model (Tkatchenko et al., 2013). Compared to the range-separated self-consistently screened (rsSCS) variant of MBD (Ambrosetti et al., 2014b), the use of the VV polarizability functional enables consistent treatment of ionic compounds, normalization to the free-atom reference balances the accuracy of the VV polarizability across the periodic table, and normalization to jellium enables effective modeling of metals and their surfaces (Ruiz et al., 2012). The construction of the new model involves a similar level of empiricism as that of MBD@rsSCS—we remove the need for tabulated reference vdW radii and for the short-range screening, while introducing a mechanism to avoid double counting of electron correlation in near-uniform density regions. We demonstrate on a series of benchmark calculations that our new model enables for the first time a consistent and reliable treatment of vdW interactions in molecular, covalent, ionic, metallic, and hybrid metal-organic systems.

We note that some of the problems of MBD@rsSCS have been previously investigated and improved upon by Gould et al. (2016). In particular, their fractionally ionic variant of MBD@rsSCS uses iterative Hirshfeld partitioning in combination with a piecewise linear dependence of atomic polarizability on charge, together with a rescaling scheme that deals with the divergence of the MBD Hamiltonian for highly polarizable systems. Our approach is instead based on a general polarizability functional.

Atomic models, such as MBD, require an atomic response model in the form of static polarizabilities $\alpha_{0,i}$ and $C_{6,ii}$ coefficients. In MBD-NL, we parametrize the response of atoms by coarse-graining the VV polarizability density to atomic fragments (Hirshfeld, 1977; Sato and Nakai, 2009, 2010). The VV polarizability functional is a semilocal functional of the electron density $n(\mathbf{r})$, which models the local isotropic dynamic polarizability density,

$$\alpha^{\mathrm{VV}}[n](\mathbf{r}, \mathrm{i}u) = \frac{n(\mathbf{r})}{\frac{4\pi}{3} n(\mathbf{r}) + C \frac{|\nabla n(\mathbf{r})|^4}{n(\mathbf{r})^4} + u^2} \tag{1}$$

*Emails: science@jan.hermann.name, alexandre.tkatchenko@uni.lu

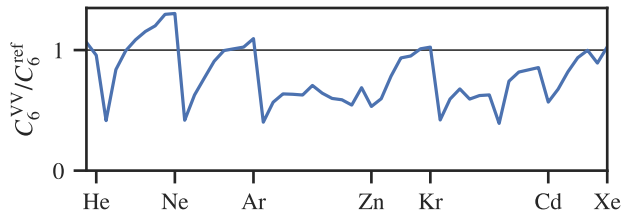

Figure 1 | Relative errors in C_6 coefficients of free atoms calculated with the VV polarizability functional for the first 54 elements of the periodic table. The reference values are the same as those used in the TS method (Tkatchenko and Scheffler, 2009).

where iu is imaginary frequency and C is an empirical parameter. The atomic dynamic polarizabilities are obtained by partitioning the polarizability density with Hirshfeld weights $w_i^{\mathrm{H}}(\mathbf{r})$,

$$\alpha_i^{\mathrm{VV}}(\mathrm{i}u) = \int \mathrm{d}\mathbf{r}\; w_i^{\mathrm{H}}(\mathbf{r})\alpha^{\mathrm{VV}}[n](\mathbf{r}, \mathrm{i}u) \tag{2}$$

The C_6 coefficients are then calculated directly from $\alpha_i(\mathrm{i}u)$ via the Casimir–Polder formula,

$$C_{6,ii}^{\mathrm{VV}} = \frac{3}{\pi}\int_0^\infty \mathrm{d}u\; \alpha_i^{\mathrm{VV}}(\mathrm{i}u)^2 \tag{3}$$

Unlike in approaches that use Hirshfeld fragments to define atomic volumes, the particular choice of the atomic partitioning in MBD-NL is inconsequential, because it only influences local redistribution of the polarizability between atoms, conserving the total polarizability. Our approach is also different from that of Silvestrelli (2008), in which the electron density is coarse-grained first and a polarizability functional is evaluated over those fragment densities.

Already this initial combination of the MBD model and VV polarizability functional gives a substantial improvement in description of ionic systems over MBD@rsSCS, owing to the versatility of the VV functional. However, it suffers from two fundamental shortcomings. First, the polarizability functional is not guaranteed to be accurate for atoms across the periodic table. Second, when combined with semilocal density-functional theory (DFT), it suffers from double counting of electron correlation in regions of slowly-varying electron density. To solve these two challenges, we normalize the atomic VV polarizabilities and C_6 coefficients to reproduce the respective exact quantities for free atoms, as motivated by the TS model (Tkatchenko and Scheffler, 2009), and then normalize MBD-NL to give zero vdW energy for jellium by subtracting the portion of the polarizability that comes from slowly-varying electron-density regions.

The VV polarizability functional is only approximate, which is manifest already for free-atom polarizabilities and C_6 coefficients, where accurate reference values are known (Figure 1). Especially the polarizabilities and C_6 coefficients of atoms of metallic elements are substantially underestimated. To mitigate this error, we normalize the VV atomic quantities with the ratio of the free-atom polarizabilities and C_6 coefficients as calculated by the VV functional and as obtained from accurate reference calculations,

$$\alpha_{0,i}^{\mathrm{rVV}} = \alpha_{0,i}^{\mathrm{VV}}\frac{\alpha_{0,i}^{\mathrm{ref,free}}}{\alpha_{0,i}^{\mathrm{VV,free}}}, \quad C_{6,i}^{\mathrm{rVV}} = C_{6,i}^{\mathrm{VV}}\frac{C_{6,i}^{\mathrm{ref,free}}}{C_{6,i}^{\mathrm{VV,free}}} \tag{4}$$

This scaling assumes that any error in the VV functional is transferable from free atoms to atoms in compounds.

Many exchange–correlation (XC) functionals are exact for jellium by construction, even though the portion of electron correlation coming from the nonlocal plasmons is long-ranged and should not be accounted for by semilocal XC functionals. As a result of this construction, most XC functionals describe accurately the electron correlation *within* slowly-varying density regions, such as those found in metals, and no addition of vdW forces is needed in those cases. This is different in most general systems, in which semilocal functionals neglect long-range vdW interactions. At the same time, these metallic-density regions contribute dominantly to the polarizability in the VV functional (in principle the local polarizability of a conductor should be infinite) and hence to the vdW energy in any vdW model, in which the VV functional would be used directly. When combined with semilocal DFT, this would result in overpolarization and overbinding of bulk metals as well as of adsorbates on metallic surfaces. To avoid this double counting, the VV10 expression for the vdW energy subtracts the limit of the VV10 nonlocal functional as the density gradient approaches zero,

$$E_{\mathrm{vdW}}^{\mathrm{VV10}} = E^{\mathrm{VV10}}[n] - \left(E^{\mathrm{VV10}}|_{\boldsymbol{\nabla} n\to 0}\right)[n] \tag{5}$$

Such an approach cannot be used directly in a many-body model such as MBD, because unlike in a pairwise model the many-body vdW energy is not linear in the polarizability.

To ensure the correct zero limit of MBD-NL for uniform electron densities, we smoothly cut off the contribution of jellium-like regions to the polarizability. These regions can be distinguished using the combination of two local electron-density descriptors: the local ionization potential I (Gutle et al., 1999) and the iso-orbital indicator χ (Becke and Edgecombe, 1990; Kümmel and Perdew, 2003; Sun et al., 2013),

$$I[n] = \tau^{\mathrm{W}}[n]/n, \qquad \chi[n] = \frac{\tau^{\mathrm{KS}}[n] - \tau^{\mathrm{W}}[n]}{\tau^{\mathrm{unif}}[n]} \tag{6}$$

where $\tau[n] = \sum_i |\boldsymbol{\nabla}\phi_i|^2/2$ is the positive kinetic energy density of occupied orbitals ϕ_i, which for single-orbital densities reduces to the von Weizsäcker kinetic energy density, $\tau^{\mathrm{W}}[n] = |\boldsymbol{\nabla} n|^2/8n$, and for jellium to $\tau^{\mathrm{unif}}[n] = 3(3\pi^2)^{2/3}n^{5/3}/10$. The local ionization potential is a form of a reduced gradient with the units of energy, which attempts to model the local electronic gap. The density gradient alone is not sufficient to characterize metallic density. In particular, both $I \sim 0$ and $\chi \sim 1$ must be true for density to be metallic, whereas $I \sim 0$ and $\chi \sim 0$ corresponds to centers of covalent bonds (dominated by a single bonding orbital), and $I \sim 0$ and $\chi \gg 1$ signifies overlaps of electron-density tails that occur between noncovalently bound systems. Since the normalization of VV10 to jellium uses only the density gradient, it partially omits also contributions from covalent bonds. By using also the iso-orbital indicator, we make MBD-NL more precise in this regard.

Figure 2a presents polarizability density distributions of I and χ in three benzene compounds and in a set of simple solids (Zhang et al., 2018). In an organic molecule such as benzene (Figure 2a), the vast majority of the polarizability comes from electron density with $I > 5\,\mathrm{eV}$ while a small part comes from

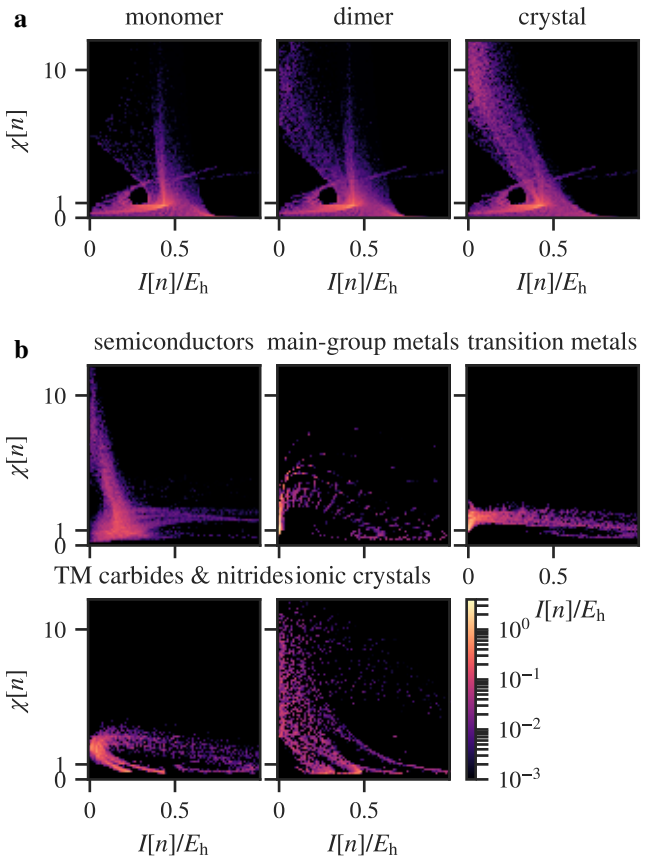

Figure 2 | Polarizability distributions of local ionization potential I and iso-orbital indicator χ. Precisely, the plotted distributions are $\alpha^{\mathrm{VV}}(s',\chi') = \int \mathrm{d}\mathbf{r}\delta(s(\mathbf{r})-s')\delta(\chi(\mathbf{r})-\chi')\alpha^{\mathrm{VV}}(\mathbf{r})$, such that the total polarizability is equal to $\iint \mathrm{d}s\mathrm{d}\chi\, \alpha^{\mathrm{VV}}(s,\chi)$. (**a**) Benzene monomer, dimer, and crystal. Each distribution is normalized to one benzene molecule. (**b**) 64 simple solids divided to five groups (Zhang et al., 2018). Each distribution is normalized to 62 (a. u.), the VV polarizability of a benzene monomer, to share a single color scale with **a**.

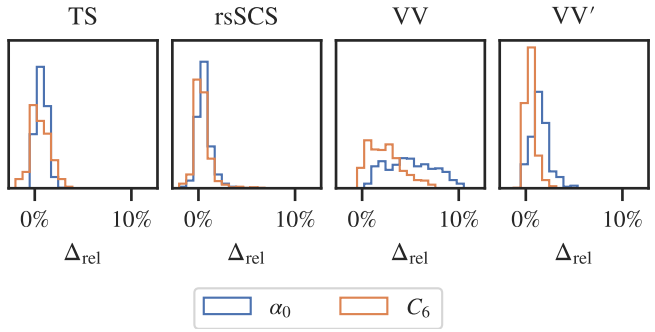

Figure 3 | Distributions of relative changes in atomic polarizabilities and C_6 coefficients from monomers to dimers. The distributions are calculated over all atoms from all complexes in the S66 data set (Řezáč et al., 2011).

low-gradient regions with $\chi < 1$. With the introduction of intermolecular interactions in the benzene dimer and crystal, a significant additional amount of polarizability comes from regions with $\chi \gg 1$, despite the electron density being low in such regions. A richer spectrum of patterns can be found in simple solids (Figure 2b). Most similar to the benzene compounds is the group of semiconductors. In contrast, the vast majority of the polarizability in main-group metals comes from jellium-like regions near $(I,\chi) = (0,1)$. In transition metals, the polarizability is distributed over a wider range of the local gap along the $1 < \chi < 2$ strip, with a larger part still coming from the low-gradient regions. In simple ionic solids, most of the polarizability comes from single-orbital regions ($\chi < 1$).

To avoid the double counting of vdW interactions of low-gradient density regions, we smoothly cut off their contribution to the polarizability functional,

$$\alpha^{\mathrm{VV}'}[n](\mathbf{r}) = g(I,\chi)\alpha^{\mathrm{VV}}[n] \tag{7}$$

We impose two simple requirements on this cutoff. First, the density regions with a local gap lower than the work function of jellium (< 5 eV) should not contribute to the calculated vdW energy, because those are assumed to be covered by a semilocal XC functional. Second, the VV polarizability of simple covalent compounds (exemplified by a benzene molecule) should not be influenced by the cutoff. The following function g satisfies these two requirements:

$$g(I,\chi) = 1 - \frac{1 - f\big(\chi - 3\sqrt{I}\big)}{1 + \exp\big(4(I - 5\,\mathrm{eV})/1\,\mathrm{eV}\big)}, \qquad f(x) = \exp\big(-cx/(1-x)\big)\theta(1-x) \tag{8}$$

Function g is composed from a logistic damping function centered at 5 eV with the width of 1 eV, and function f is taken from the SCAN functional (Sun et al., 2015), where it also serves to interpolate between $\chi = 0$ and $\chi = 1$. We find that $c = 0.1$ ensures that the effect of the cutoff on the VV polarizability of a benzene molecule is negligible (< 2%).

Apart from avoiding the double counting of long-range electron correlation in low-gradient regions, the cutoff function removes another deficiency of the VV polarizability functional. When molecules are brought together to form vdW-bound compounds, the introduction of density-tail overlaps significantly increases the polarizability when using a model such as the VV functional (Figure 2a). This effect is an artifact of the VV functional that causes increasingly large vdW-bound systems to be overbound, and cutting off the polarizability of low-gradient regions with $\chi > 1$ eliminates this issue without affecting the polarizabilities of isolated monomers compounds (Figure 3).

Finally, the static polarizabilities and C_6 coefficients calculated as described above are directly used in the MBD Hamiltonian to obtain the vdW energy. The MBD Hamiltonian describes a system of charges in harmonic potentials—Drude oscillators—characterized by their static polarizabilities $\alpha_{0,i}$ and resonance frequencies $\omega_i = 4C_{6,ii}/3\alpha_{0,i}^2$, and interacting via a long-range dipole potential $\mathbf{T}^{\mathrm{lr}}(\mathbf{R}) \equiv f_{\mathrm{lr}}(R)\mathbf{T}(\mathbf{R})$,

$$H^{\mathrm{MBD}}(\{\alpha_{0,i},\omega_i\}) = \sum_i -\frac{1}{2}\nabla^2_{\xi_i} + \sum_i \frac{1}{2}\omega_i^2\xi_i^2 + \frac{1}{2}\sum_{ij}\omega_i\omega_j\sqrt{\alpha_{0,i}\alpha_{0,j}}\boldsymbol{\xi}_i\cdot\mathbf{T}^{\mathrm{lr}}_{ij}\boldsymbol{\xi}_j \tag{9}$$

where $\boldsymbol{\xi}_i \equiv \sqrt{m_i}\mathbf{x}_i$ are mass-weighted displacements of the charges. The interaction energy of this model system—the vdW

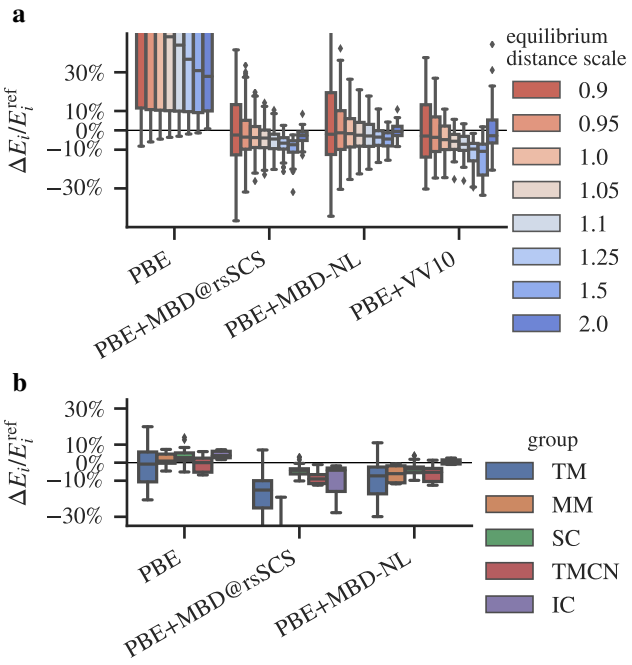

Figure 4 | Distributions of relative errors in binding and lattice energies. (**a**) S66×8 set of organic dimers. The scale encoded by the color multiplies the equilibrium distance between the centers of mass of two given monomers. (**b**) Set of 64 hard solids (Zhang et al., 2018). The color encodes the class of a solid: transition metals (TM), main-group metals (MM), semiconductors (SC), transition-metal carbides and nitrides (TMCN), and ionic crystals (IC).

energy—is obtained by direct diagonalization resulting in a set of coupled oscillation frequencies $\tilde{\omega}_k$,

$$E_{\mathrm{MBD}} = \sum_{k}^{3N} \frac{\tilde{\omega}_k}{2} - \sum_{i}^{N} \frac{3\omega_i}{2} \tag{10}$$

In MBD-NL, we use the same form of the long-range coupling $\mathbf{T}^{\mathrm{lr}}$ as in the MBD@rsSCS variant (Ambrosetti et al., 2014b), but with a simplified definition of the vdW radii. Rather than using tabulated vdW radii, we use the quantum-mechanical formula for vdW radii of free atoms from Fedorov et al. (2018), which are scaled with the ratios of VV polarizability of an atom in a compound and that of a free atom,

$$R_i^{\mathrm{vdW}} = \tfrac{5}{2}(\alpha_{0,i}^{\mathrm{ref,free}})^{\frac{1}{7}} \left(\frac{\alpha_i^{\mathrm{rVV'}}}{\alpha_i^{\mathrm{rVV',free}}} \right)^{\frac{1}{3}} \tag{11}$$

We optimize the damping parameter β of $f_{\mathrm{lr}}(R)$ on the S66 data set (Řezáč et al., 2011), as was done for MBD@rsSCS, and find the optimal values of 0.81 and 0.83 for the XC functionals PBE (Perdew et al., 1996) and PBE0 (Adamo and Barone, 1999), respectively, only slightly smaller than the optimal values of 0.83 and 0.85 for MBD@rsSCS.

Next, we briefly describe several benchmark tests of the MBD-NL model (see Appendix for a more detailed description of the calculations and additional results). The performance of MBD-NL on a set of small organic dimers (S66, Řezáč et al., 2011) is nearly identical to that of MBD@rsSCS (Figure 4a), which is already excellent for a DFT+vdW approach. In contrast, the errors in lattice energies of 64 hard solids (Zhang et al., 2018) are reduced drastically when MBD@rsSCS is replaced by MBD-NL (Figure 4b). This improvement comes mainly from the errors on metals and ionic solids, which PBE+MBD@rsSCS overbinds substantially, whereas plain PBE performs reasonably well, and MBD-NL even slightly improves upon it. PBE+MBD-NL still somewhat overbinds the metals compared to PBE, but this can be expected, because bare PBE does not underbind the metals despite the missing (non-jellium) long-range vdW interactions. Ionic solids are underbound by 4% with PBE, which is reduced nearly to zero when the missing nonlocal correlation is added by MBD-NL, whereas MBD@rsSCS overbinds some of the ionic solids substantially. The performance of MBD-NL on semiconductors is similar to that of MBD@rsSCS. On a set of organic molecular crystals (X23, Reilly and Tkatchenko, 2013), the performance of MBD-NL is identical to MBD@rsSCS, with a similar tendency to underbind (2%) as that of MBD@rsSCS to overbind (3%). On a set of supramolecular complexes (S12L, Grimme, 2012), the accuracy of PBE+MBD-NL is reduced compared to PBE+MBD@rsSCS, going from 5% to 9% in terms of the mean absolute relative error (MARE), but the accuracy of the two methods is equal with the PBE0 functional, with MBD-NL having a smaller mean relative error compared to MBD@rsSCS.

Compounds with small or zero electronic gap pose the hardest problem for DFT+vdW approaches, because in principle such systems require long-range coupling of delocalized electronic fluctuations. Despite that, MBD-NL reaches the accuracy of established effective models for hybrid interfaces of metallic surfaces and organic molecules, such as the MBD@rsSCS[surf] method (Ruiz et al., 2016), with a difference in the binding energy between the two methods below 10% for a benzene molecule on a silver (111) surface. This is possible because the long-wavelength electronic fluctuations in the metal have no correlation counterpart in the adsorbed molecule, so the fully delocalized treatment of the fluctuations is in fact not necessary in this case. In contrast, the delocalized fluctuations cannot be effectively neglected in layered vdW materials with small band gaps, such as the transition-metal dichalcogenides (TMDCs), which comprise 23 of the benchmark set of 26 layered materials (here dubbed "26", Björkman, 2012). MBD@rsSCS and VV10 overbind the "26" set by 10% and 52%, respectively, indicating that both models overpolarize these small-gap layered compounds. In contrast, the nonlocal part of the polarizability generated by low-gradient density regions is removed in MBD-NL, resulting in its underbinding of the "26" set by 21% (the accuracy of the reference calculations is 10%–20%). Of the three methods, the three non-TMDC layered materials in the "26" set (graphite, BN, PbO) are described most accurately by MBD-NL (MARE of 7%, compared to 27% for MBD@rsSCS and 53% for VV10).

Before concluding, we discuss some of the potential future improvements of MBD-NL. First, the VV polarizability functional is semi-empirical and it can be improved by including nonlocal density information, for example by developing a meta-GGA polarizability functional. Another possible improvement would be to normalize the vdW parameters not only to free atoms, but also to ions (Gould et al., 2016). Second, although MBD-NL can effectively treat hybrid interfaces between organic and metallic compounds, it does not capture the truly nonlocal electronic fluctuations that can be found in conductors (Dobson, 2014). Incor-

porating such a mechanism would not only enable MBD-NL to treat long-range interactions between fully metallic bodies, but also increase its accuracy for interacting systems of small-gap compounds, as shown here on the case of TMDCs. Third, MBD-NL uses an empirical range-separating function parameterized for a given XC functional. Developing seamless range separation approaches that couple semilocal XC functionals and vdW methods remains an open challenge (Hermann and Tkatchenko, 2018).

In conclusion, we have developed a vdW model that unifies atomic many-body approaches and nonlocal vdW functionals. By normalizing to free atoms and jellium, we have retained the accuracy of best DFT+vdW approaches while extending applicability to ionic and metallic compounds and hybrid metal-organic interfaces. Our approach enables efficient, accurate, and consistent modeling of many-body vdW interactions in a substantially broader range of systems than previously possible.

Appendix

All computational resources for the manuscript can be found in a Git repository (Hermann, 2019a) and related data files (Hermann, 2019b). This includes scripts used to generate input files, to run the calculations, process and analyze data, and generate figures. The file organization is described in the `README.md` file in the repository.

All DFT calculations were done with FHI-aims (Blum et al., 2009), which uses atom-centered basis sets with numerical radial parts. We used the `tight` default basis set and grid settings, which ensure numerical convergence to 0.1 kcal/mol in binding energies for the van der Waals (vdW) systems studied here. MBD calculations were performed with the help of the Libmbd library (Hermann, 2019c), which is integrated into FHI-aims, and MBD-NL calculations can be performed directly in FHI-aims with a current development version. The PBE, PBE0, and VV10 energies for the S66, X23, and S12L sets were taken from (Hermann and Tkatchenko, 2018), which used the same numerical settings as this work. For molecular crystals, k-point grids with density of at least 0.8 Å in reciprocal space were used for all DFT and MBD calculations. For hard solids, we have used the k-point density from (Zhang et al., 2018). All molecular and crystal geometries were taken directly from the respective benchmark sets without any relaxation.

Table 1 reports the performance of MBD-NL, MBD@rsSCS, and VV10, in combination with the PBE and PBE0 functionals, on the set of organic molecular crystals (X23, Reilly and Tkatchenko, 2013), a set of supramolecular complexes (S12L, Grimme, 2012), and a set of 26 layered materials (dubbed "26", Björkman, 2012). Of the standard vdW data sets, S12L is the only one where PBE and PBE0 differ in performance. This results mostly from PBE binding the π–π complexes somewhat more than PBE0. The proper balance between semilocal DFT and long-range vdW models in the case of large π–π complexes is unclear (Hermann and Tkatchenko, 2018). On the "26" set, the MBD@rsSCS Hamiltonian has negative eigenvalues for 20 of the 26 compounds. To obtain finite energies nevertheless, we use the eigenvalue rescaling as proposed by Gould et al. (2016).

Figure 5 compares the binding energy curve of a hybrid organic/inorganic interface as calculated by PBE-NL and surface variants of the MBD@rsSCS and TS methods by Ruiz et al. (2016).

Table 1 | Errors in interaction energies on vdW benchmark data sets.

method		S66	X23	S12L	"26"[a]
PBE	MRE[b]	57%	60%	82%	105%
+MBD@rsSCS	MARE[c]	8.4%	6.4%	5.3%	(14%)[d]
	MRE	−3.1%	−3.4%	−1.4%	(−10%)
+MBD-NL	MARE	9.3%	6.2%	9.2%	21%
	MRE	−0.1%	1.9%	6.4%	21%
+VV10	MARE	9.9%	15%	15%	(52%)[e]
	MRE	−6.1%	−15%	−15%	(−52%)
PBE0	MRE	56%	58%	75%	
+MBD@rsSCS	MARE	7.6%	5.4%	6.5%	
	MRE	−1.1%	−1.7%	−4.4%	
+MBD-NL	MARE	8.5%	5.7%	6.8%	
	MRE	0.0%	3.0%	1.7%	
+VV10	MARE	8.3%	15%	20%	
	MRE	−5.3%	−15%	−20%	

[a]Data set of interlayer binding energies of 26 layered materials with RPA benchmark energies by Björkman et al. (2012). [b]Mean relative error. Negative numbers indicate overbinding. [c]Mean absolute relative error. [d]The eigenvalue rescaling for MBD by Gould et al. (2016) must be used, otherwise the MBD Hamiltonian has nonnegative eigenvalues for only 6 compounds (graphite, BN, PbO, and 3 TMDCs). [e]Results as given by Björkman (2012) for the original PW86r+VV10 combination.

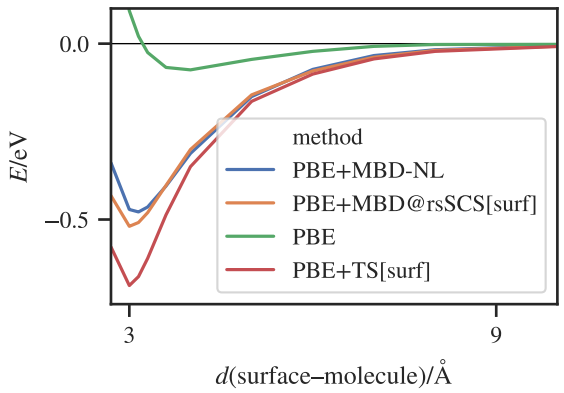

Figure 5 | Binding energy of a single benzene molecule on a (111) silver surface.

References

C. Adamo and V. Barone. Toward reliable density functional methods without adjustable parameters: The PBE0 model. *J. Chem. Phys.*, 110(13):6158–6170, Mar. 1999. doi:10.1063/1.478522.

A. Ambrosetti, D. Alfè, R. A. DiStasio, Jr., and A. Tkatchenko. Hard Numbers for Large Molecules: Toward Exact Energetics for Supramolecular Systems. *J. Phys. Chem. Lett.*, 5(5):849–855, Mar. 2014a. doi:10.1021/jz402663k.

A. Ambrosetti, A. M. Reilly, R. A. DiStasio, Jr., and A. Tkatchenko. Long-range correlation energy calculated from coupled atomic response functions. *J. Chem. Phys.*, 140(18):18A508, May 2014b. doi:10.1063/1.4865104.

A. D. Becke and K. E. Edgecombe. A simple measure of electron localization in atomic and molecular systems. *J. Chem. Phys.*, 92(9):5397–5403, May 1990. doi:10.1063/1.458517.

A. D. Becke and E. R. Johnson. Exchange-hole dipole moment and the dispersion interaction revisited. *J. Chem. Phys.*, 127(15):154108, Oct. 2007. doi:10.1063/1.2795701.

T. Björkman. Van der Waals density functional for solids. *Phys. Rev. B*, 86(16): 165109, Oct. 2012. doi:10.1103/PhysRevB.86.165109.

T. Björkman, A. Gulans, A. V. Krasheninnikov, and R. M. Nieminen. Van der Waals Bonding in Layered Compounds from Advanced Density-Functional

First-Principles Calculations. *Phys. Rev. Lett.*, 108(23):235502, June 2012. doi:10.1103/PhysRevLett.108.235502.

V. Blum, R. Gehrke, F. Hanke, P. Havu, V. Havu, X. Ren, K. Reuter, and M. Scheffler. Ab initio molecular simulations with numeric atom-centered orbitals. *Comput. Phys. Commun.*, 180(11):2175–2196, Nov. 2009. doi:10.1016/j.cpc.2009.06.022.

E. Caldeweyher, S. Ehlert, A. Hansen, H. Neugebauer, S. Spicher, C. Bannwarth, and S. Grimme. A generally applicable atomic-charge dependent London dispersion correction. *J. Chem. Phys.*, 150(15):154122, Apr. 2019. doi:10.1063/1.5090222.

M. Dion, H. Rydberg, E. Schröder, D. C. Langreth, and B. I. Lundqvist. Van der Waals density functional for general geometries. *Phys. Rev. Lett.*, 92(24): 246401, June 2004. doi:10.1103/PhysRevLett.92.246401.

J. F. Dobson. Beyond pairwise additivity in London dispersion interactions. *Int. J. Quantum Chem.*, 114(18):1157–1161, Sept. 2014. doi:10.1002/qua.24635.

D. V. Fedorov, M. Sadhukhan, M. Stöhr, and A. Tkatchenko. Quantum-Mechanical Relation between Atomic Dipole Polarizability and the van der Waals Radius. *Phys. Rev. Lett.*, 121(18):183401, Nov. 2018. doi:10.1103/PhysRevLett.121.183401.

T. Gould, S. Lebègue, J. G. Ángyán, and T. Bučko. A Fractionally Ionic Approach to Polarizability and van der Waals Many-Body Dispersion Calculations. *J. Chem. Theory Comput.*, 12(12):5920–5930, Dec. 2016. doi:10.1021/acs.jctc.6b00925.

S. Grimme. Supramolecular Binding Thermodynamics by Dispersion-Corrected Density Functional Theory. *Chem. Eur. J.*, 18(32):9955–9964, Aug. 2012. doi:10.1002/chem.201200497.

S. Grimme, J. Antony, S. Ehrlich, and H. Krieg. A consistent and accurate ab initio parametrization of density functional dispersion correction (DFT-D) for the 94 elements H-Pu. *J. Chem. Phys.*, 132(15):154104, Apr. 2010. doi:10.1063/1.3382344.

S. Grimme, A. Hansen, J. G. Brandenburg, and C. Bannwarth. Dispersion-Corrected Mean-Field Electronic Structure Methods. *Chem. Rev.*, 116(9): 5105–5154, May 2016. doi:10.1021/acs.chemrev.5b00533.

C. Gutle, A. Savin, J. B. Krieger, and J. Chen. Correlation energy contributions from low-lying states to density functionals based on an electron gas with a gap. *Int. J. Quantum Chem.*, 75(4-5):885–888, Jan. 1999. doi:10.1002/(SICI)1097-461X(1999)75:4/5<885::AID-QUA53>3.0.CO;2-F.

J. Hermann. MBD-NL: Code. 2019a. doi:10.6084/m9.figshare.9943361.v2. (git repository).

J. Hermann. MBD-NL: Data. 2019b. doi:10.6084/m9.figshare.9943301.v1. (data in HDF5 format).

J. Hermann. Libmbd. 2019c. doi:10.5281/zenodo.3474093. (git repository).

J. Hermann and A. Tkatchenko. Electronic exchange and correlation in van der Waals systems: Balancing semilocal and nonlocal energy contributions. *J. Chem. Theory Comput.*, 14(3):1361–1369, Feb. 2018. doi:10.1021/acs.jctc.7b01172.

J. Hermann, R. A. DiStasio, Jr., and A. Tkatchenko. First-principles models for van der Waals interactions in molecules and materials: Concepts, theory, and applications. *Chem. Rev.*, 117(6):4714–4758, Mar. 2017. doi:10.1021/acs.chemrev.6b00446.

F. L. Hirshfeld. Bonded-atom fragments for describing molecular charge densities. *Theoret. Chim. Acta*, 44(2):129–138, June 1977. doi:10.1007/BF00549096.

R. L. Jaffe. Casimir effect and the quantum vacuum. *Phys. Rev. D*, 72(2):021301, July 2005. doi:10.1103/PhysRevD.72.021301.

J. Klimeš and A. Michaelides. Perspective: Advances and challenges in treating van der Waals dispersion forces in density functional theory. *J. Chem. Phys.*, 137(12):120901, Sept. 2012. doi:10.1063/1.4754130.

S. Kümmel and J. P. Perdew. Two avenues to self-interaction correction within Kohn–Sham theory: Unitary invariance is the shortcut. *Mol. Phys.*, 101(9): 1363–1368, May 2003. doi:10.1080/0026897031000094506.

F. London. Zur Theorie und Systematik der Molekularkräfte [On theory and classification of molecular forces]. *Z. Physik*, 63(3-4):245–279, Mar. 1930. doi:10.1007/BF01421741.

D. Lu, Y. Li, D. Rocca, and G. Galli. Ab initio Calculation of van der Waals Bonded Molecular Crystals. *Phys. Rev. Lett.*, 102(20):206411, May 2009. doi:10.1103/PhysRevLett.102.206411.

J. P. Perdew, K. Burke, and M. Ernzerhof. Generalized Gradient Approximation Made Simple. *Phys. Rev. Lett.*, 77(18):3865–3868, Oct. 1996. doi:10.1103/PhysRevLett.77.3865.

A. M. Reilly and A. Tkatchenko. Understanding the role of vibrations, exact exchange, and many-body van der Waals interactions in the cohesive properties of molecular crystals. *J. Chem. Phys.*, 139(2):024705, July 2013. doi:10.1063/1.4812819.

J. Řezáč, K. E. Riley, and P. Hobza. S66: A Well-balanced Database of Benchmark Interaction Energies Relevant to Biomolecular Structures. *J. Chem. Theory Comput.*, 7(8):2427–2438, Aug. 2011. doi:10.1021/ct2002946.

V. G. Ruiz, W. Liu, E. Zojer, M. Scheffler, and A. Tkatchenko. Density-Functional Theory with Screened van der Waals Interactions for the Modeling of Hybrid Inorganic-Organic Systems. *Phys. Rev. Lett.*, 108(14):146103, Apr. 2012. doi:10.1103/PhysRevLett.108.146103.

V. G. Ruiz, W. Liu, and A. Tkatchenko. Density-functional theory with screened van der Waals interactions applied to atomic and molecular adsorbates on close-packed and non-close-packed surfaces. *Phys. Rev. B*, 93(3):035118, Jan. 2016. doi:10.1103/PhysRevB.93.035118.

T. Sato and H. Nakai. Density functional method including weak interactions: Dispersion coefficients based on the local response approximation. *J. Chem. Phys.*, 131(22):224104, Dec. 2009. doi:10.1063/1.3269802.

T. Sato and H. Nakai. Local response dispersion method. II. Generalized multicenter interactions. *J. Chem. Phys.*, 133(19):194101, Nov. 2010. doi:10.1063/1.3503040.

P. L. Silvestrelli. Van der Waals Interactions in DFT Made Easy by Wannier Functions. *Phys. Rev. Lett.*, 100(5):053002, Feb. 2008. doi:10.1103/PhysRevLett.100.053002.

P. L. Silvestrelli. Van der Waals interactions in density functional theory by combining the quantum harmonic oscillator-model with localized Wannier functions. *J. Chem. Phys.*, 139(5):054106, Aug. 2013. doi:10.1063/1.4816964.

J. Sun, B. Xiao, Y. Fang, R. Haunschild, P. Hao, A. Ruzsinszky, G. I. Csonka, G. E. Scuseria, and J. P. Perdew. Density Functionals that Recognize Covalent, Metallic, and Weak Bonds. *Phys. Rev. Lett.*, 111(10):106401, Sept. 2013. doi:10.1103/PhysRevLett.111.106401.

J. Sun, A. Ruzsinszky, and J. P. Perdew. Strongly Constrained and Appropriately Normed Semilocal Density Functional. *Phys. Rev. Lett.*, 115(3):036402, July 2015. doi:10.1103/PhysRevLett.115.036402.

A. Tkatchenko and M. Scheffler. Accurate Molecular Van Der Waals Interactions from Ground-State Electron Density and Free-Atom Reference Data. *Phys. Rev. Lett.*, 102(7):073005, Feb. 2009. doi:10.1103/PhysRevLett.102.073005.

A. Tkatchenko, R. A. DiStasio, Jr., R. Car, and M. Scheffler. Accurate and Efficient Method for Many-Body van der Waals Interactions. *Phys. Rev. Lett.*, 108(23): 236402, June 2012. doi:10.1103/PhysRevLett.108.236402.

A. Tkatchenko, A. Ambrosetti, and R. A. DiStasio, Jr. Interatomic methods for the dispersion energy derived from the adiabatic connection fluctuation-dissipation theorem. *J. Chem. Phys.*, 138(7):74106, Feb. 2013. doi:10.1063/1.4789814.

O. A. Vydrov and T. Van Voorhis. Nonlocal van der Waals Density Functional Made Simple. *Phys. Rev. Lett.*, 103(6):063004, Aug. 2009. doi:10.1103/PhysRevLett.103.063004.

O. A. Vydrov and T. Van Voorhis. Nonlocal van der Waals density functional: The simpler the better. *J. Chem. Phys.*, 133(24):244103, Dec. 2010a. doi:10.1063/1.3521275.

O. A. Vydrov and T. Van Voorhis. Dispersion interactions from a local polarizability model. *Phys. Rev. A*, 81(6):062708, June 2010b. doi:10.1103/PhysRevA.81.062708.

J. Yang, W. Hu, D. Usvyat, D. Matthews, M. Schütz, and G. K.-L. Chan. Ab initio determination of the crystalline benzene lattice energy to sub-kilojoule/mole accuracy. *Science*, 345(6197):640–643, Aug. 2014. doi:10.1126/science.1254419.

G.-X. Zhang, A. M. Reilly, A. Tkatchenko, and M. Scheffler. Performance of various density-functional approximations for cohesive properties of 64 bulk solids. *New J. Phys.*, 20(6):063020, 2018. doi:10.1088/1367-2630/aac7f0.